Journal of ELECTRONIC MATERIALS, Vol. 41, No. 11, 2012
DOI: 10.1007/s11664-012-2203-6

Undercooling Behavior and Intermetallic Compound Coalescence in Microscale Sn-3.0Ag-0.5Cu Solder Balls and Sn-3.0Ag-0.5Cu/Cu Joints

M.B. ZHOU,[1] X. MA,[1] and X.P. ZHANG[1,2]

1.—School of Materials Science and Engineering, South China University of Technology, Guangzhou 510640, China. 2.—e-mail: mexzhang@scut.edu.cn

The microstructure of microscale solder interconnects and soldering defects have long been known to have a significant influence on the reliability of electronic packaging, and both are directly related to the solidification behavior of the undercooled solder. In this study, the undercooling behavior and solidification microstructural evolution of Sn-3.0Ag-0.5Cu solder balls with different diameters (0.76 mm, 0.50 mm, and 0.30 mm) and the joints formed by soldering these balls on Cu open pads of two diameters (0.48 mm and 0.32 mm) on a printed circuit board (PCB) substrate were characterized by differential scanning calorimetry (DSC) incorporated into the reflow process. Results show that the decrease in diameter of the solder balls leads to an obvious increase in the undercooling of the balls, while the undercooling of the solder joints shows a dependence on both the diameter of the solder balls and the diameter ratio of solder ball to Cu pad (i.e., D_s/D_p), and the diameter of the solder balls has a stronger influence on the undercooling of the joints than the dimension of the Cu pad. Coarse primary intermetallic compound (IMC) solidification phases were formed in the smaller solder balls and joints. The bulk Ag_3Sn IMC is the primary solidification phase in the as-reflowed solder balls. Due to the interfacial reaction and dissolution of Cu atoms into the solder matrix, the primary Ag_3Sn phase can be suppressed and the bulk Cu_6Sn_5 IMC is the only primary solidification phase in the as-reflowed solder joints.

Key words: Undercooling, size effect, intermetallic compound, microstructure, lead-free solder

INTRODUCTION

In electronic packaging, the microstructure of solder interconnects and the soldering defects have a significant influence on the reliability of the packaging systems, and the microstructure and mechanical properties of solder interconnects undergoing interfacial reaction during the soldering process are significantly different from those of bulk solders.[1,4] In recent years, with continuous miniaturization of consumer electronics, there has been increasing demand for high reliability of lead-free solder interconnects whose size has been scaled down gradually. It has been well recognized that material property data obtained from bulk solders are no longer reliable for reliability estimation of microscale soldered interconnects when the volume of the solder interconnect is smaller than 10^{-3} mm^3, being nearly equivalent to a solder joint of 110 μm diameter and thickness.[2,3]

Generally, the microstructure and defects in solder joints are directly related to the solidification behavior of the undercooled solder during the soldering process. Some previous studies[5,8] focused on the solder (droplet) size effect on the undercooling behavior and indicated that the degree of undercooling increases with decreasing size of the solder,

(Received October 24, 2011; accepted July 13, 2012; published online August 8, 2012)

and the scatter of the values of the undercooling also becomes larger when the size of the solders gets smaller. In addition, it was shown that the degree of undercooling was significantly influenced by trace alloying elements, such as Ni, Zn, Mn, Co, and Ti;[9,11] in particular, elements with hexagonal closed-packed (hcp) crystal structure, such as Zn, Co, and Ti, can greatly enhance the heterogeneous nucleation of β-Sn and thus significantly reduce the undercooling of the solder alloys.[11] Another way to promote the heterogeneous nucleation of β-Sn is to enhance the wetting and interfacial reaction between the solder alloy and the metallic substrate, such as Cu, Ni, and Co.[8,12,14]

However, in contrast with the many studies about the relationship among the lead-free solder's composition, soldering process conditions, microstructural evolution, and properties of the soldered joints,[15,19] relatively little is known about the undercooling behavior of microsized solder melt on metallic substrate and its influence on the solidification microstructural evolution of microscale solder interconnects during the soldering process. In particular, there is a serious lack of clear understanding of the mechanism of the solder size effect on the undercooling-dependent solidification behavior of microscale solder balls and joints, as well as on their subsequent microstructural evolution.

In this study, a differential scanning calorimetry (DSC) method was used to investigate the melting and solidification behavior of solder balls and joints with different dimensions; further, the DSC equipment, which is capable of high-precision temperature control and excellent reproducibility of the thermal cycle, was employed to simulate the reflow process, and the undercooling-dependent solidification behavior and subsequent microstructural evolution of the microscale solder balls and their joints were characterized systematically.

EXPERIMENTAL PROCEDURES

In the present study, commercially available Sn-3.0Ag-0.5Cu (wt.%) solder balls with different diameters of 0.76 mm, 0.50 mm, and 0.30 mm, and bismaleimide triazine (BT) epoxy-based printed circuit board (PCB) substrate with solder mask defined Cu open pads of 0.32 mm and 0.48 mm diameter were used. The undercooling behavior and solidification microstructure of Sn-3.0Ag-0.5Cu solder balls and Sn-3.0Ag-0.5Cu/Cu single-sided joints were investigated using a differential scanning calorimeter (DSC, Q200; TA) incorporated into the reflow process. Solder joints with different diameter ratios of solder ball to Cu pad (i.e., D_s/D_p, where D_s is the diameter of the solder ball and D_p is the diameter of the Cu pad) of 0.76/0.48, 0.50/0.48, and 0.50/0.32 were prepared by reflowing in DSC. Twenty identical samples of each type of solder ball and joint were tested to obtain reliable data. Before DSC reflow testing, the solder ball and Cu open pad surface were covered by commercial no-clean flux, and then placed in a standard high-purity (99.99%) aluminum pan for DSC reflow testing. The flux was used for improving the soldering quality of the solder joint samples and removing the samples' surface oxide layer, which may act as heterogeneous nucleation sites and influence the solidification undercooling measurement. During DSC reflow testing, both the heating and cooling rates were kept 20°C/min and the peak reflow temperature was set to 260°C; when the temperature reached the peak value, the sample was held for 1 min. To clarify the influence of the cooling rate on the solder balls' undercooling behavior, a slow cooling rate of 1°C/min and a fast cooling rate of 60°C/min were also used to conduct DSC reflow testing for the solder balls of different diameters. During the DSC reflow process, the sample was under a protective atmosphere of high-purity (≥99.999%) nitrogen gas flowing at a rate of 50 mL/min.

After DSC reflow testing, both the as-reflowed solder balls and joints were mounted in epoxy resin and well prepared for metallographic study. To enable comprehensive observation of the microstructure, a slice-and-view method was employed, in which the observation was performed on four cross-sectional planes by dividing the hemisphere into four quarters along the radial direction as illustrated in Fig. 1. An optical microscope (DM2500P; Leica) was used to examine the microstructure of the as-reflowed solder ball and joint samples, and a scanning electronic microscope (SEM, Quanta200; FEI) equipped with an energy-dispersive spectrometer (EDS, INCAPentaFET- × 3; Oxford) was used to examine the microstructure and local composition of the as-reflowed samples.

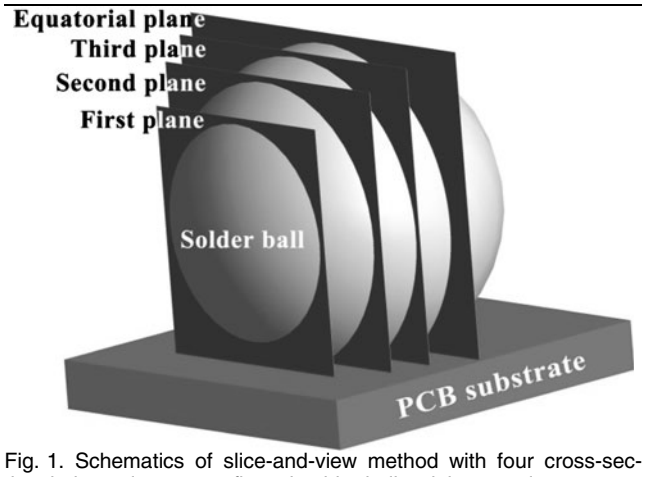

Fig. 1. Schematics of slice-and-view method with four cross-sectional planes in an as-reflowed solder ball or joint sample.

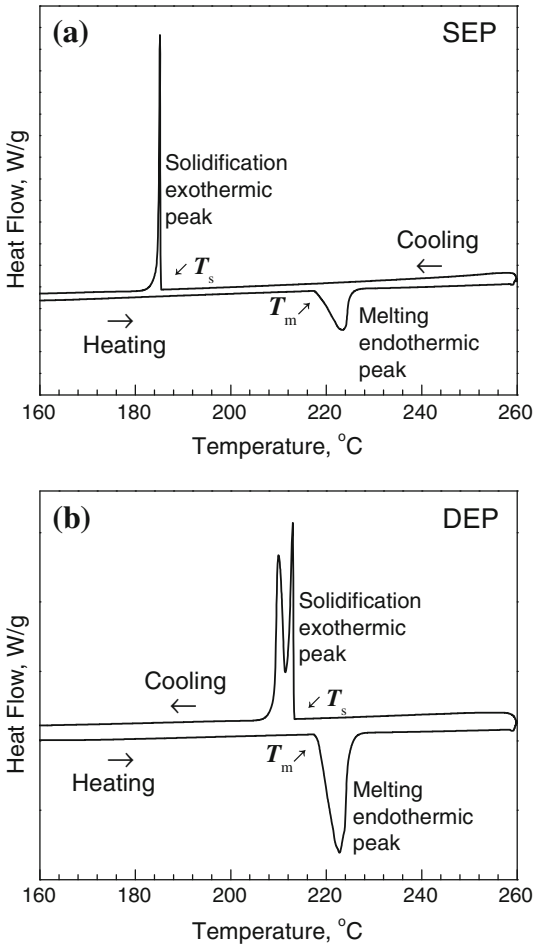

Fig. 2. Two types of DSC curves: (a) with only a single exothermic peak (SEP) on cooling, and (b) with double exothermic peaks (DEP) on cooling.

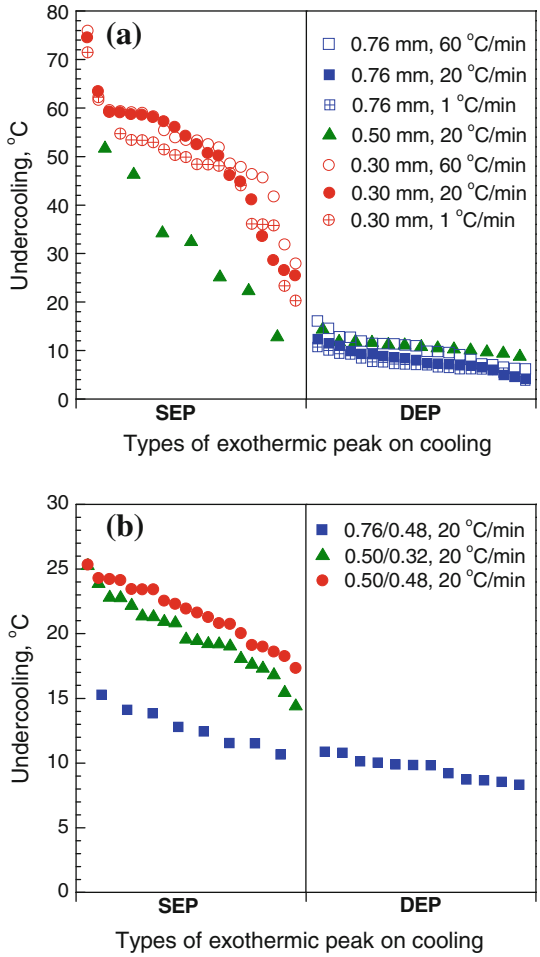

Fig. 3. Distribution of undercooling values of solder balls (a) and joints (b) with different dimensions for SEP- and DEP-type DSC curves.

RESULTS AND DISCUSSION

Undercooling Behavior of the Solder Balls and Joints

Representative DSC curves of the solder balls and joints are shown in Fig. 2, which can be divided into two types; i.e., the first type exhibits a single endothermic peak on heating and only a single exothermic peak (SEP) on cooling (i.e., during solidification; Fig. 2a), while the second type of DSC curve shows a single endothermic peak on heating and double exothermic peaks (DEP) on cooling (Fig. 2b). The undercooling (ΔT) is defined as the temperature gap between the melting onset temperature (T_m) and the solidification onset temperature (T_s).[20]

Figure 3 shows the distribution of the undercooling values of the solder balls and joints with different dimensions and having both SEP and DEP features. As shown in Fig. 3a, the solder balls with diameter of 0.30 mm exhibit only SEP feature whereas the 0.76-mm-diameter solder balls display only DEP feature. It is interesting to note that the cooling rate does not change the feature of the DSC curve, i.e., the two different types of DSC curve on cooling, SEP and DEP, are not influenced by the cooling rate. In contrast, the solder balls with diameter of 0.50 mm possess both SEP and DEP features during DSC reflow testing at cooling rate of 20°C/min. In Fig. 3b, it is clear that the solder joints with D_s/D_p ratios of 0.50/0.48 and 0.50/0.32 show only SEP feature on cooling, whereas those with D_s/D_p ratio of 0.76/0.48 display both SEP and DEP features during the DSC reflow process at cooling rate of 20°C/min. Comparing the data in Fig. 3a and 3b, clearly the solder ball and joint samples with SEP feature have significantly higher undercooling values than those with DEP feature.

Based on the data shown in Fig. 3, we can calculate the variation of the undercooling values of the solder balls and joints with different dimensions after DSC reflow testing at cooling rate of 20°C/min. Clearly, the decrease in diameter of Sn-3.0Ag-0.5Cu solder balls, from 0.76 mm to 0.50 mm then to 0.30 mm, brings about an obvious increase in the value of the undercooling; for example, the average value of the undercooling of the 0.30-mm-diameter

solder balls is 50.0°C, dropping to 8.1°C for the 0.76-mm-diameter solder balls. Furthermore, the scatter of the experimental data of the undercooling values is significantly influenced by the diameter of the solder balls. Solder balls with smaller diameter show relatively larger scatter in the undercooling values compared with larger ones. Further, using the data shown in Fig. 3, we can also calculate the average undercooling values of the solder balls after DSC reflow testing at different cooling rates. The results show that the average undercooling value of the solder balls decreases slightly as the cooling rate decreases; for example, the mean values of the undercooling for the 0.30-mm-diameter solder balls when using cooling rates of 60°C/min, 20°C/min, and 1°C/min are 52.2°C, 50.0°C, and 47.3°C, respectively, and 10.3°C, 8.1°C, and 7.0°C, respectively, for the 0.76-mm-diameter solder balls.

Interestingly, the undercooling of the solder joints shows a dependence on the diameter of the solder balls and the D_s/D_p ratio, as shown in Fig. 3b; clearly the undercooling value of the solder joints increases with decreasing diameter of the solder balls, the solder joints with D_s/D_p ratio of 0.76/0.48 have the smallest undercooling value, and the joints with D_s/D_p ratio of 0.50/0.48 show the highest undercooling value. Moreover, it can be seen that the decrease in diameter of the solder balls from 0.76 mm to 0.50 mm has a distinct influence on the undercooling value of the solder joints, in spite of the fact that the two types of solder ball were reflowed on Cu pads of constant diameter of 0.48 mm; that is, the average value of the undercooling was increased from 10.9°C for the solder joints with D_s/D_p ratio of 0.76/0.48°C to 21.6°C for the solder joints having D_s/D_p ratio of 0.50/0.48. However, the dimension of the Cu pad has only a slight influence on the undercooling of the solder joints; for example, the joints with two different D_s/D_p ratios of 0.50/0.48 and 0.50/0.32 have very similar average undercooling values of 21.6°C and 19.8°C, respectively. This means that the diameter of the solder balls has a stronger influence on the undercooling behavior of the solder joints than the dimension of the Cu pad.

Based on the undercooling results, clearly there is a strong size effect on the solidification and undercooling behavior of the solder balls and joints. According to classical solidification theory, the homogeneous nucleation rate, N, is given by[21]

$$N = K_s \exp\left[-\frac{16\pi\gamma_{sl}^3 T_m^2}{3kL_v^2 T_s \Delta T^2}\right], \quad (1)$$

where K_s is a complex function that depends on the vibration frequency of the atoms, the activation energy for diffusion in the liquid, and the surface area of the critical nuclei,[22] γ_{sl}, is the interfacial energy between crystal nuclei and the liquid, L_v is the melting enthalpy per volume, and k is the Boltzmann constant.

Assuming that at least one nucleation event is necessary to initiate solidification, for the case of volume nucleation[23]

$$NVt = 1, \quad (2)$$

where $V = 1/6\pi d^3$ expresses the volume of the metal droplet (in which d is the diameter of the metal droplet), and t is the observation time, under the condition of a constant cooling rate r, the observation time t can be replaced by $\Delta T/r$. Thus, one obtains

$$d^3 = \frac{6r}{\pi K_s \Delta T} \exp\left[\frac{16\pi\gamma_{sl}^3 T_m^2}{3kL_v^2 T_s \Delta T^2}\right]. \quad (3)$$

If the metal droplet solidifies with a heterogeneous nucleation mechanism, then the above relationship can be changed to

$$d^3 = \frac{6r}{\pi K_s \Delta T} \exp\left[\frac{16\pi\gamma_{sl}^3 T_m^2 f(\theta)}{3kL_v^2 T_s \Delta T^2}\right], \quad (4)$$

where $f(\theta)$ is the catalytic potency factor.

According to Eqs. 3 and 4, the undercooling value is closely related to the droplet dimension and the cooling rate. For a constant cooling rate (r), the undercooling value (ΔT) should increase with decreasing diameter (d) or volume (V) of the metal droplet. When the droplet diameter (d) remains constant, the undercooling value (ΔT) decreases with decreasing cooling rate (r). Clearly, the validity of the theoretical prediction described by Eqs. 3 and 4 is verified by the experimental results as shown in Fig. 3.

Microstructural Evolution of the Solder Balls and Joints

Figure 4 shows the slice-and-view microstructure on the first to equatorial cross-sectional planes of the two solder balls of 0.30 mm and 0.50 mm diameter after DSC reflow testing at cooling rate of 20°C/min, which exhibit SEP feature and have corresponding undercooling values of 50.2°C and 46.2°C, respectively. Clearly, the large bulk primary solidification phase, which was confirmed to be Ag_3Sn IMC by EDS analysis, formed in both of the as-reflowed solder balls. For comparison, Fig. 5 presents the cross-sectional microstructure of the two solder balls of 0.50 mm and 0.76 mm diameter after DSC reflow testing at cooling rate of 20°C/min, which show DEP feature and have small values of undercooling of 9.6°C and 6.1°C, respectively. Apparently, there is no large bulk primary solidification phase in either of the as-reflowed solder balls. A detailed comparison of the microstructural feature between Figs. 4 and 5 shows that the as-reflowed solder balls with SEP feature exhibit smaller grain size of the β-Sn phase and contain less amount of the eutectic phase than those with DEP feature.

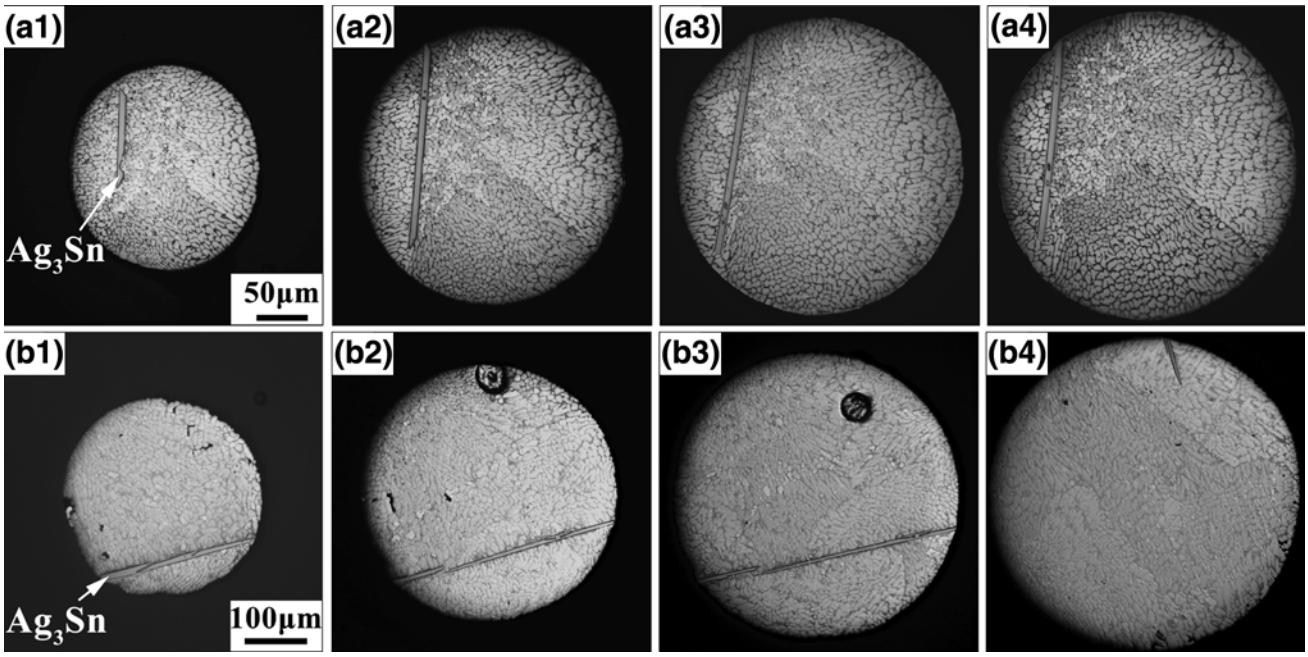

Fig. 4. Slice-and-view microstructure on the first to equatorial cross-sectional planes (i.e., a1 to a4 and b1 to b4) of the as-reflowed solder balls with SEP-type DSC curve: (a1–a4) solder ball of 0.30 mm diameter with undercooling of 50.2°C, and (b1–b4) solder ball of 0.50 mm diameter with undercooling of 46.2°C.

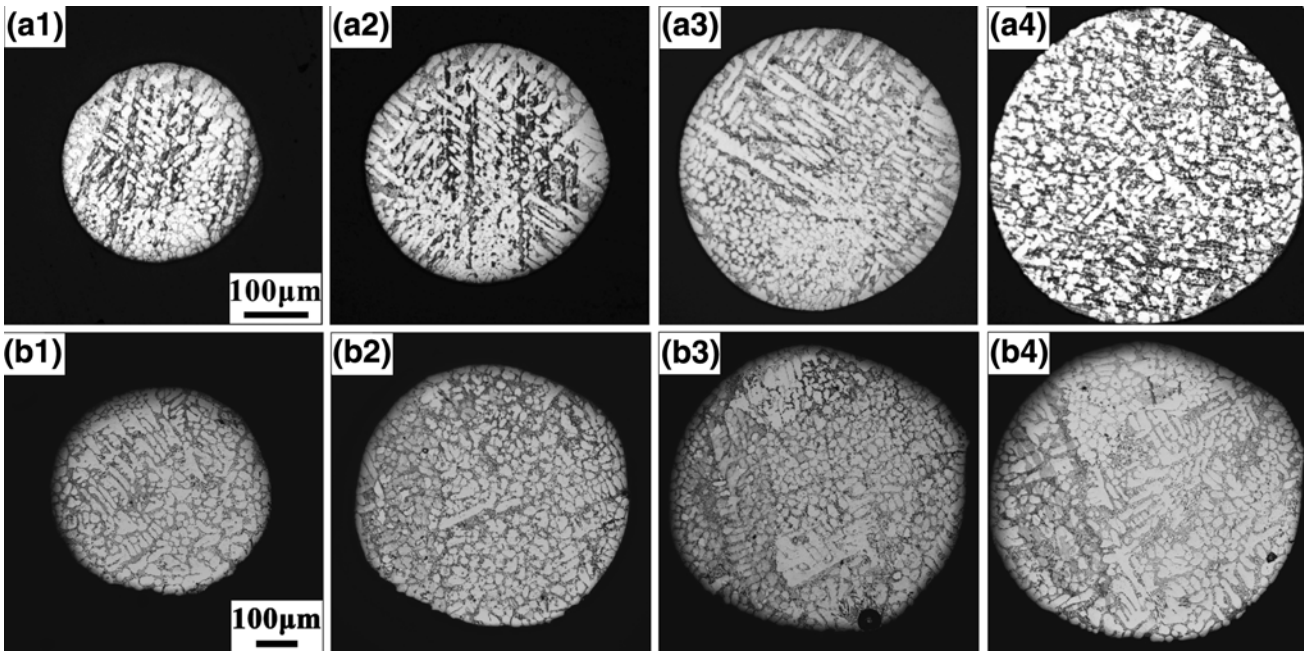

Fig. 5. Slice-and-view microstructure on the first to equatorial cross-sectional planes (i.e., a1 to a4 and b1 to b4) of the as-reflowed solder balls with DEP-type DSC curve: (a1–a4) solder ball of 0.50 mm diameter with undercooling of 9.6°C, and (b1–b4) solder ball of 0.76 mm diameter with undercooling of 6.1°C.

Clearly, the microstructural evolution of the above as-reflowed near-ternary-eutectic Sn-3.0Ag-0.5Cu solder balls with SEP feature shows that there are three kinds of phases formed in a certain sequence during nucleation and solidification; i.e., the large primary solidification phase Ag_3Sn forms first, followed by the β-Sn phase, and the eutectic phase forms at the last stage of solidification, as shown in Fig. 4. It should be indicated that, since the amount of the primary solidification phase Ag_3Sn in the samples is very small, the characteristic peak in the DSC curve corresponding to the

nucleation of the primary phase cannot be detected by DSC measurement. By contrast, the as-reflowed solder balls with DEP feature only show two kinds of microstructural phases, i.e., the first solidification phase β-Sn and the succeeding eutectic phase, as shown in Fig. 5.

Figure 6 shows the cross-sectional microstructure images on the four planes in the as-reflowed solder joints with three different D_s/D_p ratios of 0.50/0.48, 0.50/0.32, and 0.76/0.48 after DSC reflow testing at cooling rate of 20°C/min. As is known from DSC tests and the undercooling results shown in Fig. 3, all three of these types of solder joint show SEP feature, having corresponding undercooling values of 24.2°C, 16.8°C, and 15.3°C, respectively. Furthermore, it can be seen in Fig. 6 that several bulk primary solidification phases exist in each of these three solder joints. For comparison, Fig. 7 presents the microstructural evolution on the four cross-sectional planes in the solder joint with D_s/D_p ratio of 0.76/0.48 after DSC reflow testing at cooling rate of 20°C/min, which exhibits DEP feature and has an undercooling value of 9.9°C; clearly some bulk primary solidification phases also exist in the joint. The primary solidification phase in the solder joints with either SEP or DEP feature, as shown in Figs. 6 and 7, has been identified as Cu_6Sn_5 by EDS quantitative and qualitative analyses, and the qualitative analysis results of element mapping are shown in Fig. 8. Since the microstructural evolution of the adjacent cross-sectional planes shows a succession from the same sample, we can reconstruct the true morphology of the primary Cu_6Sn_5 IMC phase as rod-like through the hemisphere. This also means that we can definitely identify the compositions of the bulk primary phases by selecting EDS results in each cross-sectional plane of the solder joint. Moreover, it should be indicated that, due to diffusion of Cu atoms from the Cu pad of the PCB substrate to the solder matrix during the reflow process, the composition of the near-ternary-eutectic Sn-3.0Ag-0.5Cu solder alloy has been changed into a hypereutectic Sn-Ag-Cu alloy. Thus, the primary Cu_6Sn_5 phase can easily nucleate and grow to become a large bulk primary phase owing to the high Cu content in the hypereutectic Sn-Ag-Cu alloy, which is why we can observe clearly the bulk primary phase in both types of solder joint with large undercooling value associated with SEP feature and small undercooling values related to DEP feature, respectively. Meanwhile, it has also been shown that the solder joints with SEP feature show smaller grain size of the β-Sn phase than those with DEP feature, and these results are in good coincidence with those obtained from the solder ball samples as shown in Figs. 4 and 5.

Moreover, to clarify the variation of the undercooling behavior of the solder balls/joints with the dimension of the solder balls/joints and the type of DSC cooling curves (i.e., SEP and DEP features) as well as the microstructural characteristics of the solder balls/joints, we reprocessed the undercooling data/results shown in Fig. 3 by sorting them from high value to low value and classifying them according to the size (or dimension) of the solder balls/substrates and the primary solidification phase, as shown in Fig. 9. It is clear that the average undercooling values of the solder balls or joints with SEP feature are higher than for those with DEP feature, regardless of the solder ball dimension and the existence of the solder/substrate interface.

For the solder balls and joints with SEP feature, the primary factors controlling the undercooling behavior are the solder ball dimension and the primary solidification phase; for example, the 0.30-mm-diameter solder balls (i.e., the smallest size used in this study) with SEP feature possess the highest undercooling value of 50.0°C and the primary solidification phase of Ag_3Sn; in comparison, the 0.76/0.48 solder joints with SEP feature, which have the largest dimension of 0.76 mm, possess the lowest undercooling value of 12.8°C and the primary solidification phase of Cu_6Sn_5. The change of the primary solidification phases in the solder matrix is caused mainly by the interfacial reaction between the solder ball and Cu substrate, and can also be attributed to the dissolution of Cu atoms into the solder matrix. For the solder balls and joints with DEP feature, the primary factors influencing the undercooling behavior are the same as those for the solder balls and joints with SEP feature, i.e., the solder ball dimension and primary solidification phase, although the degree of the influence is relatively slight.

Further, the results in Fig. 9 show clearly that the undercooling of the 0.50-mm-diameter solder balls with SEP feature is higher than that of the corresponding solder joints (i.e., 0.50/0.48 and 0.50/0.32 solder/substrate). However, the undercooling of the 0.76-mm-diameter solder balls with DEP feature is less than that of the solder joints formed by the solder balls of the same dimension.

Therefore, it can be concluded that the undercooling behavior of the solder balls and joints is influenced by the coupling effect of multiple factors, which mainly include the solder ball dimension, primary solidification phases, and the interfacial heterogeneous nucleation layer; for example, although the dimension of the 0.76/0.48 solder joints with SEP feature is larger than that of the 0.50-mm-diameter solder balls with DEP feature, the undercooling value of the former is slightly greater than that of the latter. This is because the solder balls or joints of different dimensions possess different primary solidification phases, which may cause the change of the undercooling behavior.

In liquid metals, the random fluctuations in the atomic concentration can create minute unstable cluster (or embryo) regions even at temperatures higher than the melting point of the metal.[24] A previous study[25] indicated that the stability of the different clusters in the liquid alloy is greatly different. For some primary solidification phases, such as the large bulk Ag_3Sn IMC phase in the

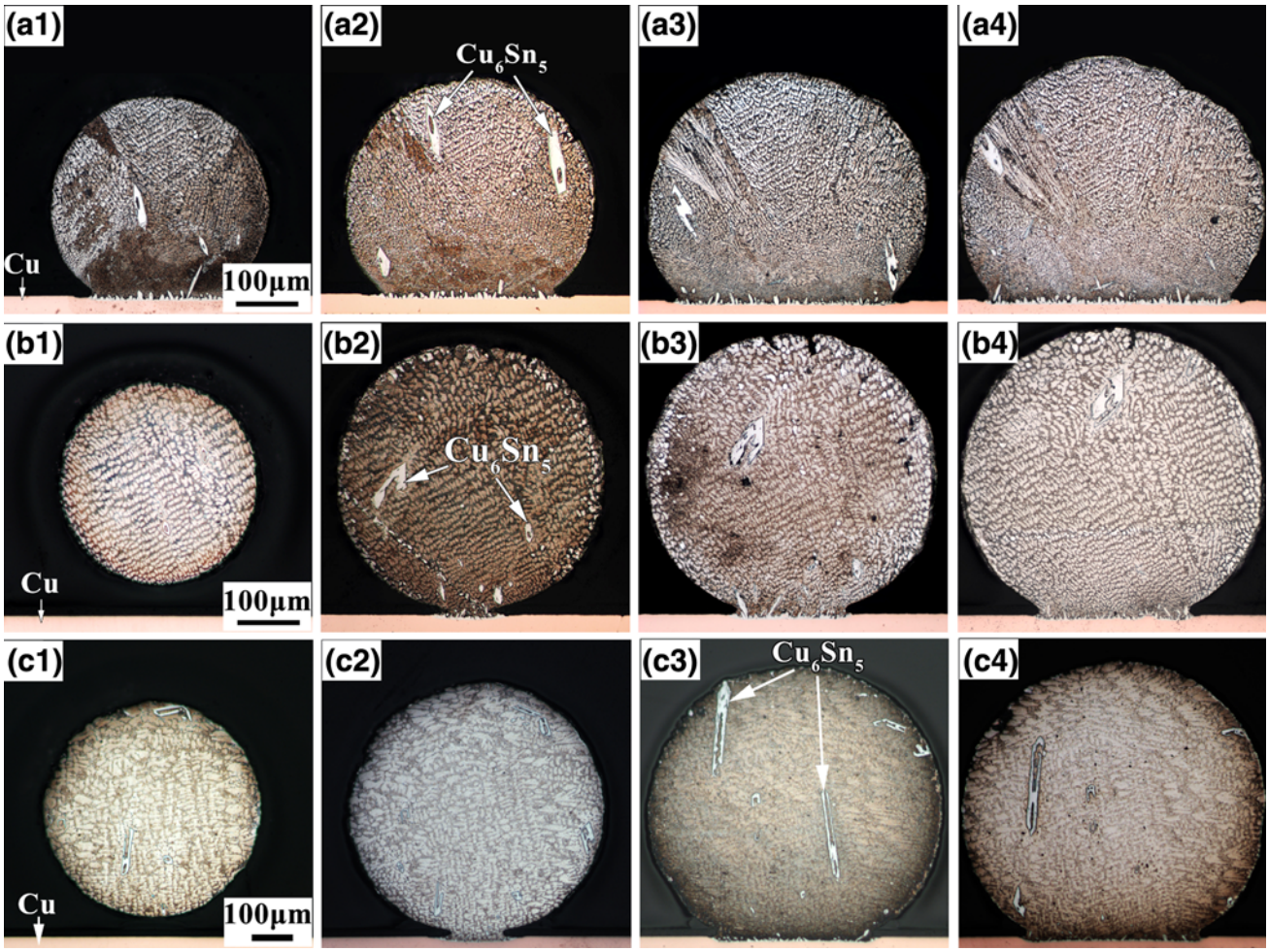

Fig. 6. Slice-and-view microstructure on the first to equatorial cross-sectional planes (i.e., a1 to a4, b1 to b4 and c1 to c4) of the as-reflowed solder joints with SEP-type DSC curve: (a1–a4) solder joint with D_s/D_p ratio of 0.50/0.48 and undercooling of 24.2°C, (b1–b4) solder joint with D_s/D_p ratio of 0.50/0.32 and undercooling of 16.8°C, and (c1–c4) solder joint with D_s/D_p ratio of 0.76/0.48 and undercooling of 15.3°C.

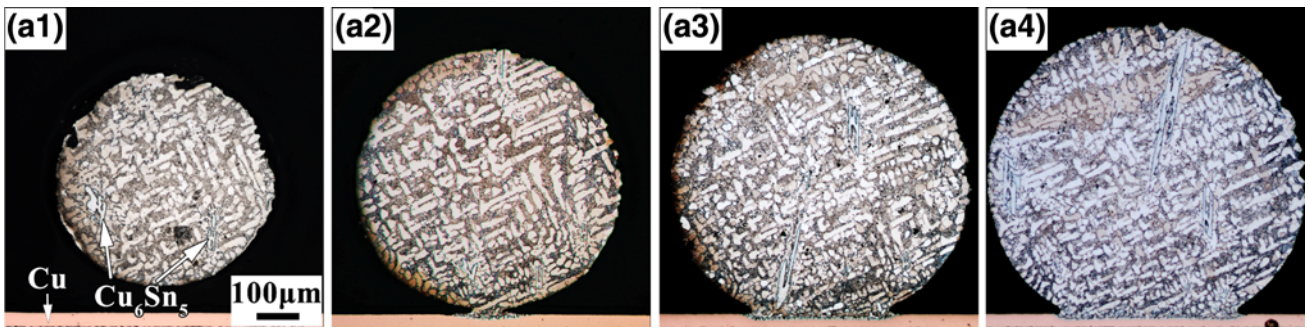

Fig. 7. Slice-and-view microstructure on the first to equatorial cross-sectional planes (i.e., a1 to a4) of the as-reflowed solder joint with D_s/D_p ratio of 0.76/0.48, DEP-type DSC curve, and undercooling of 9.9°C.

as-reflowed Sn-3.0Ag-0.5Cu solder balls, actually they would first come from the most stable clusters, in which the nucleation would occur preferably. As is shown clearly in Fig. 3, the degree of undercooling of the solder balls with SEP feature is higher than that of the balls with DEP feature, thus the solder droplets with SEP feature can exist in the molten state more easily than the solder droplets with DEP feature; further, from the atomic point of view, at the lower temperatures the clusters in the molten solder droplets with SEP feature are most likely to nucleate and solidify first, and finally grow to form the primary solidification phase, such as the primary Ag_3Sn IMC phase as shown in Fig. 4.

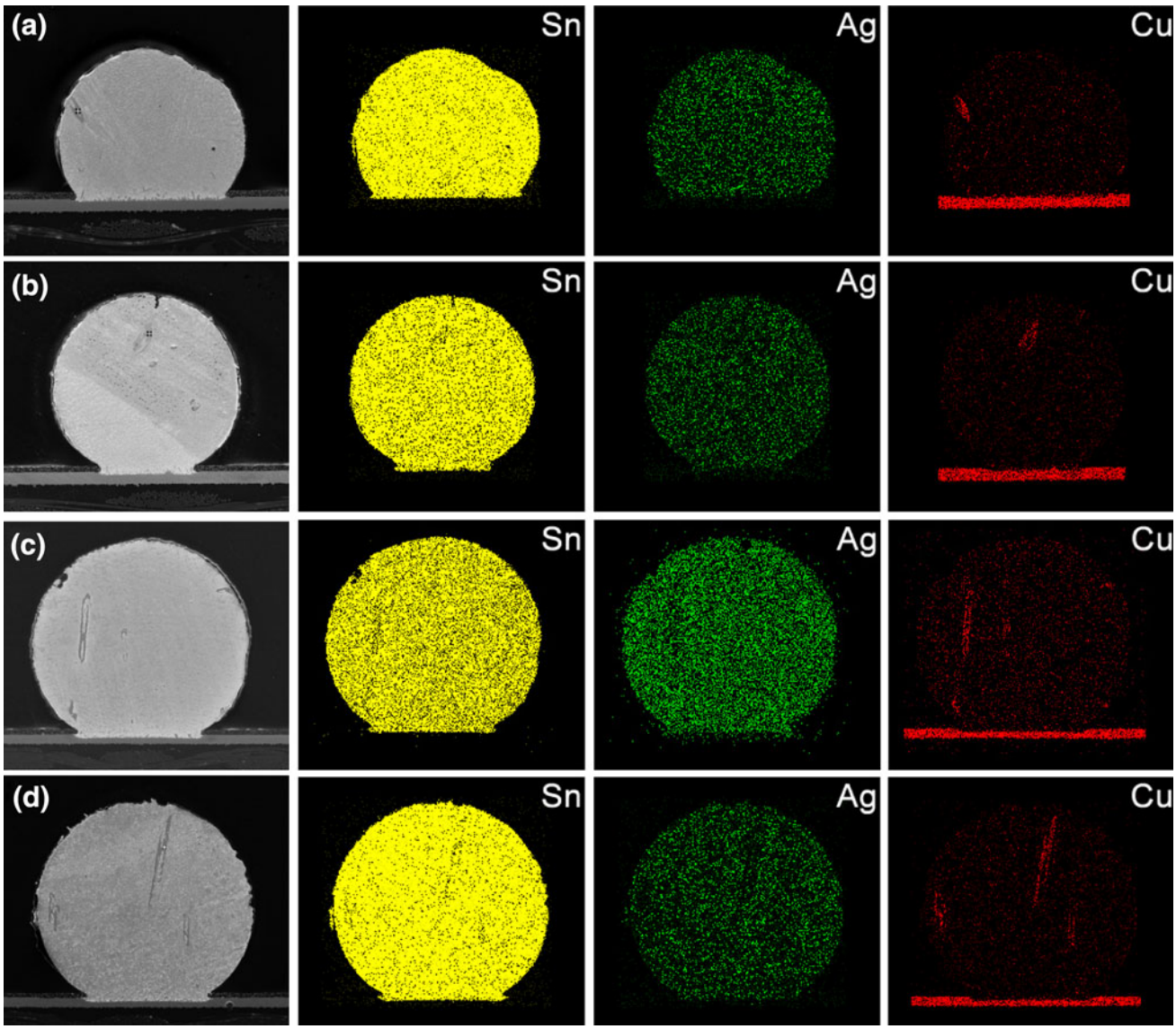

Fig. 8. Element mapping results on different cross-sectional planes: (a) Cu_6Sn_5 on the equatorial plane in Fig. 7-a4, (b) Cu_6Sn_5 on the equatorial plane in Fig. 7-b4, (c) Cu_6Sn_5 on the equatorial plane in Fig. 7-c4, and (d) Cu_6Sn_5 on the equatorial plane in Fig. 8-a4.

As is known, the degree of undercooling shows a positive correlation with the driving force for solidification during the reflow process; that is, the smaller the undercooling value, the weaker the driving force for solidification. Clearly, the solder balls or joints with DEP feature have a weaker driving force for nucleation than those with SEP feature. Accordingly, the characteristics of the solidification process of the β-Sn phase and eutectic phase in the solder balls or joints with DEP feature can be clearly correlated to the feature of the DSC curves; that is, the first exothermal peak corresponds to the easier nucleation of the β-Sn phase, and the last exothermal peak corresponds to the most difficult nucleation of the eutectic phase. By contrast, the β-Sn phase and eutectic phase in the solder balls or joints with SEP feature have a larger driving force for solidification; both of them can nucleate and solidify almost at the same time, thus there is just one exothermal peak. Since the solder balls or joints with SEP feature and a large undercooling value possess a stronger driving force for solidification than those with DEP feature and a small undercooling value, thus the β-Sn phase in the former ones nucleates much faster and solidifies within a shorter time (see Fig. 2, where constant heating and cooling rates were used), and finally the solder balls or joints exhibit much finer solidification microstructure compared with those with DEP feature. Therefore, it is naturally understandable why the solder balls or joints with SEP feature show smaller grain size of the β-Sn phase than those with DEP feature, as shown in Figs. 4 and 5. In particular, it is worth indicating that, for the solder balls with a large undercooling value, the nucleation and growth of the primary solidification Ag_3Sn phase

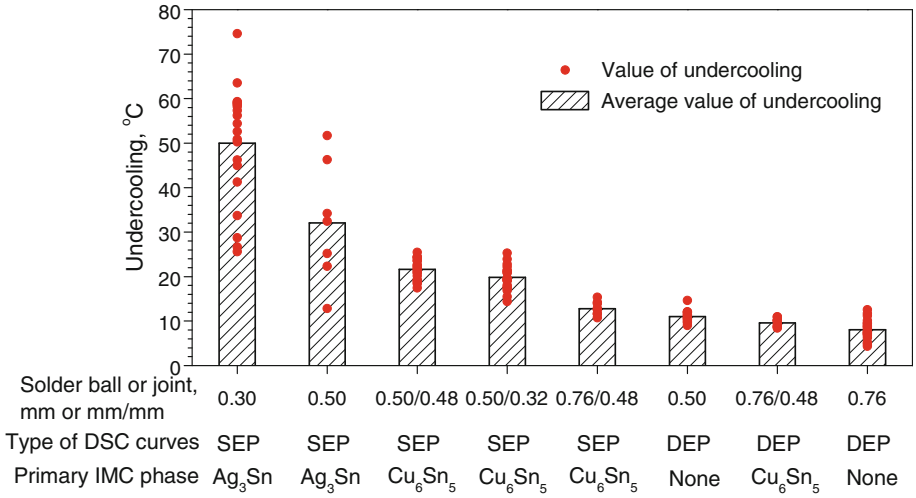

Fig. 9. Relationship of the variation of the undercooling value of the solder balls and joints with different dimensions and the type of DSC cooling curves as well as the microstructure characteristics.

result in the consumption of a large amount of Ag atoms in the solder balls during the solidification process, and thus there is an insufficient supply of Ag atoms for the formation of the succeeding eutectic phase. Thus, the as-reflowed solder balls with SEP feature (Fig. 4) contain significantly less eutectic phase than those with DEP feature (Fig. 5).

From the above results, it is clear that Ag_3Sn is the only bulk primary solidification phase in the as-reflowed Sn-3.0Ag-0.5Cu solder balls, and Cu_6Sn_5 is the only primary solidification phase in the as-reflowed Sn-3.0Ag-0.5Cu/Cu joints. Moreover, it has been shown that the interfacial reaction and the metallic substrate have a direct influence on the primary solidification product. In a previous study,[26] the thermodynamic calculation method was employed to describe the solidification process of ternary Sn-Ag-Cu solder alloys, and the results showed that different contents of Cu and Ag in the Sn-Ag-Cu alloys can significantly influence the nucleation order of the primary Cu_6Sn_5 and Ag_3Sn IMC phases; for example, the first nucleated primary phase in Sn-4.41Ag-0.63Cu alloy is Ag_3Sn, while for Sn-3.30Ag-1.47Cu alloy it is Cu_6Sn_5. According to this study, the interfacial reaction and the metallic substrate can also influence the first nucleated primary solidification phase. Due to the consumption of Cu atoms from the Cu pad and their dissolution into the solder matrix during the interfacial reaction process, the contents of Cu and Ag in the Sn-Ag-Cu solder matrix changed significantly, leading to the change of the primary solidification phase from Ag_3Sn to Cu_6Sn_5.

CONCLUSIONS

The solidification and undercooling behavior as well as the microstructural evolution of Sn-3.0Ag-0.5Cu solder balls and Sn-3.0Ag-0.5Cu/Cu joints with different dimensions were characterized by DSC reflow testing in combination with microanalysis and microstructural characterization. The results obtained have shown that:

1. There are two types of DSC curve when reflowing the solder balls and joints with different dimensions. The first type shows only a single exothermic peak (SEP) on cooling, whereas the second type exhibits double exothermic peaks (DEP) on cooling. The SEP and DEP features correspond to different solidification states of the solder balls and joints.
2. Both the solder balls and joints with SEP feature have significantly higher undercooling values and exhibit smaller grain size of the β-Sn phase than those with DEP feature. For the solder balls and joints with DEP feature, the first exothermal peak corresponds to the easier nucleation of the β-Sn phase and the last one corresponds to the most difficult nucleation of the eutectic phase.
3. The degree of undercooling of Sn-3.0Ag-0.5Cu solder balls is strongly influenced by the diameter of the balls; the decrease in diameter brings about an obvious increase of the undercooling. The undercooling of the solder joints shows a dependence on both the diameter of the solder balls and the D_s/D_p ratio, decreasing the diameter of the solder balls leads to a significant increase in the undercooling of the Sn-3.0Ag-0.5Cu/Cu joints, and the diameter of the solder balls has a stronger influence on the undercooling of the solder joints than the dimension of the Cu pad.
4. Ag_3Sn is the only bulk primary solidification phase in the as-reflowed Sn-3.0Ag-0.5Cu solder balls; the interfacial reaction and dissolution of Cu atoms into the solder matrix result in an increase of the Cu content in the solder matrix, thus the formation of the primary Ag_3Sn phase can be suppressed and Cu_6Sn_5 is the only primary solidification phase in the as-reflowed Sn-3.0Ag-0.5Cu/Cu joints.

ACKNOWLEDGMENTS

This research was supported by Research Fund for the Doctoral Program of Higher Education of China (20110172110003) and fund of the State Key Laboratory of Advanced Welding and Joining in HIT under Contract No. AWPT-Z04, and Guangdong Provincial Department of Science and Technology through the Science and Technology Major Project under Contract No. 2009A080204005.

REFERENCES

1. K.S. Kim, S.H. Huh, and K. Suganuma, *J. Alloys Compd.* 352, 226 (2003).
2. P. Zimprich, U. Saeed, A. Betzwar-Kotas, B. Weiss, and H. Ipser, *J. Electron. Mater.* 37, 102 (2008).
3. L.M. Yin, X.P. Zhang, and C. Lu, *J. Electron. Mater.* 38, 2179 (2009).
4. Y.H. Tian, C.J. Hang, C.Q. Wang, S.H. Yang, and P.R. Lin, *Mater. Sci. Eng. A* 529, 468 (2011).
5. W.B. Guan, Y.L. Gao, Q.J. Zhai, and K.D. Xu, *J. Mater. Sci.* 39, 4633 (2004).
6. R. Kinyanjui, L.P. Lehman, L. Zavalij, and E. Cotts, *J. Mater. Res.* 20, 2914 (2005).
7. Q.J. Zhai, Y.L. Gao, W.B. Guan, and K.D. Xu, *Mater. Sci. Eng. A* 441, 278 (2006).
8. Y.C. Huang, S.W. Chen, and K.S. Wu, *J. Electron. Mater.* 39, 109 (2010).
9. S.K. Kang, D.Y. Shih, D. Leonard, D.W. Henderson, T. Gosselin, S. Cho, J. Yu, and W. Choi, *JOM* 56, 34 (2004).
10. L.W. Lin, J.M. Song, Y.S. Lai, Y.T. Chiu, N.C. Lee, and J.Y. Uan, *Microelectron. Reliab.* 49, 235 (2009).
11. M.G. Cho, H.Y. Kim, S.K. Seo, and H.M. Lee, *Appl. Phys. Lett.* 95, 021905 (2009).
12. S.K. Kang, M.G. Cho, P. Lauro, and D.Y. Shih, *J. Mater. Res.* 22, 557 (2007).
13. M.G. Cho, S.K. Kang, and H.M. Lee, *J. Mater. Res.* 23, 1147 (2008).
14. M.G. Cho, S.K. Kang, S.K. Seo, D.Y. Shih, and H.M. Lee, *J. Mater. Res.* 24, 534 (2009).
15. M. Abtew and G. Selvaduray, *Mater. Sci. Eng. R* 27, 95 (2000).
16. C.M.L. Wu, D.Q. Yu, C.M.T. Law, and L. Wang, *Mater. Sci. Eng. R* 44, 1 (2004).
17. K. Zeng and K.N. Tu, *Mater. Sci. Eng. R* 38, 55 (2002).
18. K.N. Tu, A.M. Gusak, and M. Li, *J. Appl. Phys.* 93, 1335 (2003).
19. Y.C. Chan and D. Yang, *Prog. Mater Sci.* 55, 428 (2010).
20. S.W. Chen, C.C. Lin, and C. Chen, *Metall. Mater. Trans. A* 29, 1965 (1998).
21. D. Turnbull, *J. Chem. Phys.* 20, 411 (1952).
22. D.A. Porter and K.E. Easterling, *Phase Transformations in Metals and Alloys*, 2nd ed. (London: Chapman and Hall, 1992), p. 190.
23. D.M. Herlach and F. Gillessen, *J. Phys. F* 17, 1635 (1987).
24. W. Kurz and D.J. Fisher, *Fundamentals of Solidification* (Switzerland: Trans Tech publications, 1984), p. 21.
25. S. Gruner, I. Kaban, R. Kleinhempel, W. Hoyer, P. Jóvári, and R.G. Delaplane, *J. Non-Cryst. Solids* 351, 3490 (2005).
26. Y. Takamatsu, H. Esaka, and K. Shinozuka, *Mater. Sci. Forum* 654–656, 1397 (2010).